



NRC Publications Archive Archives des publications du CNRC

The influence of hydrogen enrichment on the topology of a lean, methane/air turbulent V-flame

Vena, P.; Guo, H.; Galizzi, C.; Kühni, M.; Escudié, D.

This publication could be one of several versions: author's original, accepted manuscript or the publisher's version. / La version de cette publication peut être l'une des suivantes : la version prépublication de l'auteur, la version acceptée du manuscrit ou la version de l'éditeur.

Publisher's version / Version de l'éditeur:

Digital Proceedings of 8th European Combustion Meeting, 2017-04-20

NRC Publications Record / Notice d'Archives des publications de CNRC:

<https://nrc-publications.canada.ca/eng/view/object/?id=b39b221d-319f-4c8d-b805-be3a642736a4>

<https://publications-cnrc.canada.ca/fra/voir/objet/?id=b39b221d-319f-4c8d-b805-be3a642736a4>

Access and use of this website and the material on it are subject to the Terms and Conditions set forth at

<https://nrc-publications.canada.ca/eng/copyright>

READ THESE TERMS AND CONDITIONS CAREFULLY BEFORE USING THIS WEBSITE.

L'accès à ce site Web et l'utilisation de son contenu sont assujettis aux conditions présentées dans le site

<https://publications-cnrc.canada.ca/fra/droits>

LISEZ CES CONDITIONS ATTENTIVEMENT AVANT D'UTILISER CE SITE WEB.

Questions? Contact the NRC Publications Archive team at

PublicationsArchive-ArchivesPublications@nrc-cnrc.gc.ca. If you wish to email the authors directly, please see the first page of the publication for their contact information.

Vous avez des questions? Nous pouvons vous aider. Pour communiquer directement avec un auteur, consultez la première page de la revue dans laquelle son article a été publié afin de trouver ses coordonnées. Si vous n'arrivez pas à les repérer, communiquez avec nous à PublicationsArchive-ArchivesPublications@nrc-cnrc.gc.ca.



The Influence of Hydrogen Enrichment on the Topology of a Lean, Methane/Air Turbulent V-Flame

P. Vena^{*1}, H. Guo², C. Galizzi¹, M. Kühni¹, D. Escudie¹

¹ CETHIL, Université de Lyon, CNRS, INSA Lyon, France

²Energy, Mining and Environment, National Research Council, Canada

Abstract

The influence of hydrogen enrichment on the topology of lean CH₄-H₂/air turbulent V-flames was considered. Three equivalence ratios with different levels of hydrogen enrichment were studied for variations in flame topology. The turbulent flame speed and turbulent flame brush thickness both increased with hydrogen enrichment for all flame considered. Flame surface density profiles showed a progressive shift towards the products and curvature PDFs showed a bias towards positive curvatures. Observed trends were attributed to the changes in thermo-diffusive stability of the reactants as Lewis numbers decreased with hydrogen volume fraction.

1. Introduction

Growing concerns for environmental sustainability and pollutant mitigation have lead combustion scientists to search for cleaner fuels in engineering applications. On this basis, hydrogen enriched fuel blends, where hydrogen is mixed with a conventional parent fuel, are among the more promising approaches currently being explored. When coupled with methane [1,2], natural gas [3], or gasoline [4], hydrogen enrichment has been shown to increase the thermodynamic efficiency of combustion systems and reduce gaseous emissions of CO₂, the principle greenhouse gas, as well as CO, NO_x, and particulates such as soot [5], which impact local air quality. Moreover, hydrogen enriched fuel blends (e.g. hythane, 20% hydrogen and 80% natural gas) can be accommodated within existing infrastructure [6], making them suitable for integration into a range of industrial applications and capable of having an immediate impact on current technologies.

Despite the obvious benefit of hydrogen enrichment, its application to real-world combustion systems remains limited due to practical issues (supply, storage, security), but also due to an incomplete understanding of how it influences the fundamental behavior of flames. In particular, we are still unable to accurately predict flame properties over a broad range of hydrogen/hydrocarbon fuel ratios for different equivalence ratios, turbulence intensities, and reactant temperatures and pressures, making it difficult to define the safe and effective “operational limits” of hydrogen enriched fuel blends. It is therefore imperative that we make rapid progress towards understanding the physical mechanisms induced by the intrinsic characteristics of hydrogen (diffusivity, Lewis number, etc...). Only once this has been addressed, can we effectively improve the currently oversimplified numerical tools used to develop and optimize next generation, hydrogen enriched combustion devices.

Our approach to the problem is to focus on the influence of thermal and mass diffusivities of the reactant mixture by varying the fraction of hydrogen and parent hydrocarbon. To this end, we will study turbulent, lean methane-hydrogen/air (CH₄-H₂/air) flames of equivalence ratios $\phi = 0.55$, $\phi = 0.45$, and $\phi = 0.35$ for fuel mixtures ranging from 100% methane and 0% hydrogen, to only 20% methane and 80% hydrogen. For each CH₄-H₂ fuel, we will discuss variations in flame front topology and study key combustion parameters such as turbulent flame speed S_T , turbulent flame brush thickness δ_T , flame surface density Σ , and flame front curvature κ .

The preliminary results presented here will provide experimental data that will serve as a reference for testing numerical models and validating theory, and give insight into the physical mechanisms that govern the behavior of hydrogen enriched flames.

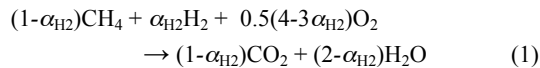
2. Experimental apparatus and methodology

Experiments were conducted on premixed, CH₄-H₂/air V-flames stabilized at the exit of a 115 x 115 mm square exit nozzle burner [7]. The CH₄, H₂, and air streams were independently regulated with Brooks mass flow controllers.

Individual flame realizations were obtained from Mie scattering images by seeding reactant air with olive oil droplets. The optical setup included a New Wave solo-12 pulsed 532 nm laser with a Rodenstock laser sheet generator. Images were acquired with a LaVision Imager proX 2048 x 2048 camera equipped with a Vincent Associates mechanical shutter (VCM-D1), a Nikon Nikkor 50 mm lens, and a bandpass filter centered at 532 nm (± 10 nm at FWHM). The analysis region of interest was between axial positions $x = 68$ -142.5 mm above the exit plane of the burner and transverse positions $y = 0$ -53.5 mm from the centerline of the burner, and images had a projected spatial resolution of 83 $\mu\text{m}/\text{pixel}$. The acquisition rate was limited to 2Hz to ensure individual flow structures were not present in consecutive images.

* Corresponding author: patrizio.vena@insa-lyon.fr

The influence of hydrogen enrichment was studied for equivalence ratios $\phi = 0.55$, $\phi = 0.45$, and $\phi = 0.35$ by varying the fuel volume fraction of hydrogen α_{H_2} by 10% increments. The methane, hydrogen, and air concentrations were calculated from the reaction equation,



following the method outlined in [7]. Table 1 summarizes experimental flame settings.

Turbulence properties were measured with a Dantec Dynamics Laser Doppler Anemometry (LDA) system at axial position $x = 10$ mm between transverse positions $y = \pm 45$ mm. Under cold flow conditions, the mean flow velocity was $U = 3.89$ m/s. Two separate perforated plates were used to generate turbulence. The measured turbulence intensities were $u'/U = 3.1\%$ and $u'/U = 6.1\%$.

Table 1 Summary of test conditions.

Equivalence ratio, ϕ^*	Volume fraction of H_2 , $\alpha_{H_2}^*$	Adiabatic flame temperature, T_{ad}^{**} [K]	Laminar flame speed, S_L^{**} [cm/s]	Lewis number, Le^{**}	u'/S_L $u' = 11.9$ and 23.7 cm/s
0.55	0.0	1570	8.01	0.91	1.49 - 2.96
	0.1	1573	8.66	0.90	1.38 - 2.73
	0.2	1580	9.47	0.89	1.26 - 2.50
	0.3	1586	10.55	0.88	1.13 - 2.24
	0.4	1596	11.98	0.87	1.00 - 1.98
0.45	0.3	1393	3.64	0.90	3.28 - 6.50
	0.4	1401	4.24	0.88	2.81 - 5.58
	0.5	1411	5.13	0.86	2.33 - 4.61
	0.6	1421	6.32	0.84	1.89 - 3.75
0.35	0.6	-	-	-	-
	0.7	1223	1.2	0.82	9.81 - 19.53
	0.8	1240	1.8	0.76	6.63 - 13.15

*The volume fraction of hydrogen was calculated from $\alpha_{H_2} = V_{H_2} / (V_{H_2} + V_{CH_4})$, where V_{H_2} and V_{CH_4} represent the volume flow rate of H_2 and CH_4 respectively.

**The adiabatic flame temperature T_{ad} , laminar flame speed S_L , and Lewis number Le (ratio of thermal diffusivity of the reactant mixture to molecular diffusivity of the deficient reactant) were calculated based on simulations of 1D laminar premixed CH_4 - H_2 /air flames in Chemkin. The simulation for case $\phi = 0.35$ $\alpha_{H_2} = 0.6$ did not result in a converged solution and was omitted.

3. Results and discussion

Five hundred individual Mie scattering images were acquired for each flame condition outlined in Table 1. Raw images were filtered using a 7×7 median filter (0.58×0.58 mm) and binarized by simple thresholding. The image complement was then calculated such that combustion products had pixel values of one and reactants had pixel values of zero (shown in Figure 1). The resulting images were used to evaluate the influence of hydrogen enrichment on the instantaneous flame topology, turbulent flame speed S_T , turbulent flame brush thickness δ_T , flame surface density Σ , and flame curvature κ .

3.1 Instantaneous flame topology

Sample instantaneous binary images are shown in Figure 1 for flames with an equivalence ratio $\phi = 0.45$, and hydrogen fraction $\alpha_{H_2} = 0.4$ and $\alpha_{H_2} = 0.6$ in (a) and (b) respectively.

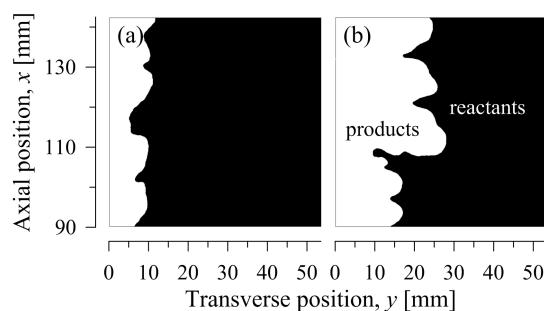


Figure 1 Instantaneous binarized Mie scattering images for $u'/U = 3.1\%$ flame conditions $\phi = 0.45$ $\alpha_{H_2} = 0.3$ in (a) and $\phi = 0.45$ $\alpha_{H_2} = 0.6$ in (b).

Through visual inspection of both images, differences in the topology and wrinkling scales of the flame front are observed. In Figure 1 (a), the flame contour is characterized by smoother structures in both positive (convex towards reactants) and negative (concave towards reactants) curvature

regions. Conversely, in Figure 1 (b), sharper, cusp-like structures protruding into the products are observed in negative curvature regions, while positive curvatures tend to extend into the reactants. This trend became more prominent as the volume fraction of H₂ was increased, and this was consistently observed for the three equivalence ratios considered.

The observed flame structures are comparable to those reported in turbulent V-flames of similar Lewis numbers Le [8,9], where differences are explained by thermo-diffusive theory [10]. In brief, competing thermal and mass diffusivities of the deficient reactant can alter flame wrinkling. In the current experiments, as Le decreases with H₂ volume fraction α_{H_2} , the relatively higher diffusive flux of the deficient reactant enhances positively curved flame regions (\uparrow flame speed) and starves negatively curved flame regions (\downarrow flame speed). This then promotes the formation of positive curvature structures that extend towards the reactants, and weaker negative curvature cusp-like structures that recede towards the products. Lewis numbers are provided in Table 1.

3.2 Turbulent Flame Speed S_T and Turbulent Flame Brush Thickness δ_T

Maps of mean reaction progress variable $\langle c \rangle$ were obtained with the ensemble average of individual binary flame images. A sample map is shown in Figure 2 (a) for flame condition $\phi = 0.55$ $\alpha_{H_2} = 0.2$, and represents the probability of the presence of the products.

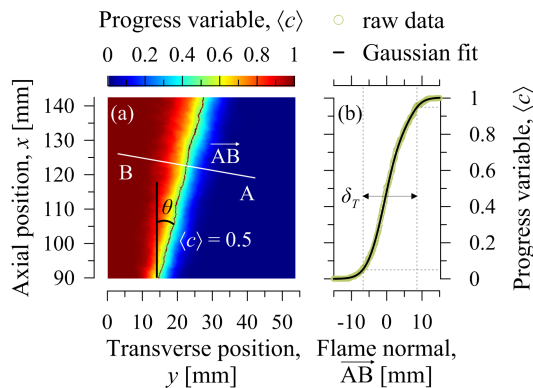


Figure 2 Sample mean reaction progress variable $\langle c \rangle$ map for flame condition $\phi = 0.55$ $\alpha_{H_2} = 0.2$ in (a) showing the $\langle c \rangle = 0.5$ iso-contour in black, flame normal \overline{AB} , and incident flame angle θ . The variation in $\langle c \rangle$ across \overline{AB} is shown in (b) and represents the turbulent flame brush profile. The Gaussian fit used to determine the turbulent flame brush thickness δ_T is also shown.

Within the map, the $\langle c \rangle = 0.5$ iso-contour corresponds to the mean position of the flame front. It has an incident angle θ from which the turbulent

flame speed $S_T = U \sin(\theta)$ is estimated (where U is the mean flow velocity).

Figure 3 plots calculated S_T in terms of the laminar flame speed S_L for turbulent flames $u'/U = 3.1\%$ in (a) and $u'/U = 6.1\%$ in (b). At equivalent ϕ and α_{H_2} , results showed a monotonic increase in S_T/S_L with u'/U . This trend was observed for all flames considered, and is consistent with the commonly accepted expression for turbulent flame speed $S_T/S_L = 1 + A(v'/S_L)^n$ [11].

Figure 3 (a) and (b) further show a general increase in S_T/S_L with hydrogen fraction α_{H_2} for the three equivalence ratios considered. While this result is inconsistent with the predicted decrease in S_T/S_L of the above expression (since S_L increases with α_{H_2}), it is in agreement with the experimental results of [7] on turbulent V-flames and the DNS results of [12]. The analysis of [7] suggests that hydrogen enrichment increases the turbulent flame speed due to both an increase in S_L (caused by chemical kinetics and stretch), in addition to a change in flame topology (turbulent flame brush thickness and total flame surface area).

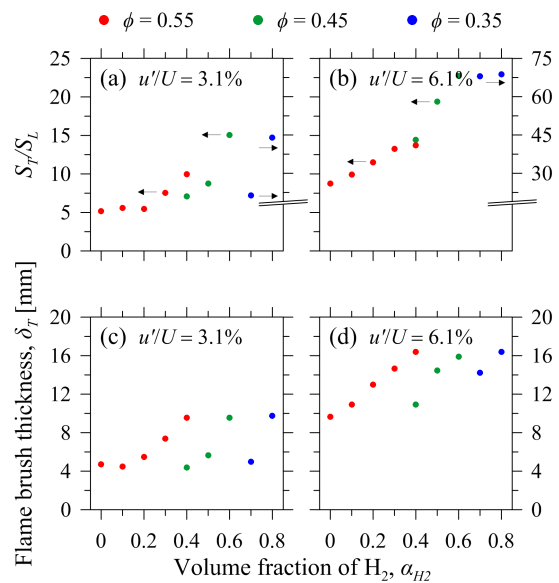


Figure 3 Comparison of the ratio S_T/S_L in (a) and (b), and of the turbulent flame brush thickness δ_T in (c) and (d) among lean CH₄-H₂/air flames for equivalence ratios $\phi = 0.55$, $\phi = 0.45$, and $\phi = 0.35$.

The turbulent flame brush thickness δ_T was measured by fitting a Gaussian function to the distribution of $\langle c \rangle$ as it varies across the flame normal \overline{AB} , shown in Figure 2 (a) and (b). It is here defined as the distance between $\langle c \rangle = 0.05$ and $\langle c \rangle = 0.95$ iso-contours.

Comparing Figure 3 (c) and (d) shows that δ_T increases monotonically with u'/U for equivalent ϕ and α_{H_2} , a trend consistent with turbulent flame theory [13].

The influence of α_{H_2} on δ_T is presented in Figure 3 (c) for weaker turbulence flames, and data show a general increase in δ_T with α_{H_2} for the three equivalence ratios considered. Matching trends were observed for weaker turbulence cases in (d).

Overall, the results of Figure 3 were in agreement with those of [7] and support their conclusion that that S_T is a function of both laminar flame speed and flame topology.

3.3 Flame Surface Density Σ

Flame surface density statistics were obtained following the approach described in [14,15], where $\Sigma = \langle \Sigma' \rangle = \langle |\nabla c| \cdot \delta(c - c_f) \rangle$. Individual binary flame images were used to determine Σ' . No attempts were made to correct for flame front orientation angle in the orthogonal plane z , such that $\Sigma' = \Sigma'_{xy} = \langle \partial L / \partial A \rangle$.

FSD profiles are shown in Figure 4 for equivalence ratios $\phi = 0.55$, $\phi = 0.45$, and $\phi = 0.35$ and turbulence intensities $u'/U = 3.1\%$ and 6.1% . All profiles are gently skewed towards the products with peak values consistently between $\langle c \rangle = 0.5-0.7$. This asymmetry is typically observed in turbulent V-

flames of comparable Lewis numbers [8], and is attributed to the presence of cusped structures of negative curvature along the flame front [16]. This was observed qualitatively through visual inspection of individual flame images (see Section 3.1), and further confirmed by the gradual shift in bias of FSD profiles in (a), (b), and (c).

In addition, a near-linear decrease in the magnitude of FSD was observed with α_{H_2} in (a), (b), and (c). This decrease coincides with the increase in turbulent flame brush thickness reported in Table 1, suggesting that the enhanced number and intensity of wrinkles with α_{H_2} is offset by the bigger increase in δ_T .

The same trends were generally observed for higher turbulence intensities in (d), (e), and (f) as profiles also showed a progressive shift towards reactants and a near-linear decrease in FSD with α_{H_2} . However, the influence of hydrogen enrichment was less obvious than for the weaker turbulence cases.

Overall, observed trends were consistent with the FSD measurements of [7] on lean $\text{CH}_4\text{-H}_2/\text{air}$ V-flames of comparable turbulence intensities.

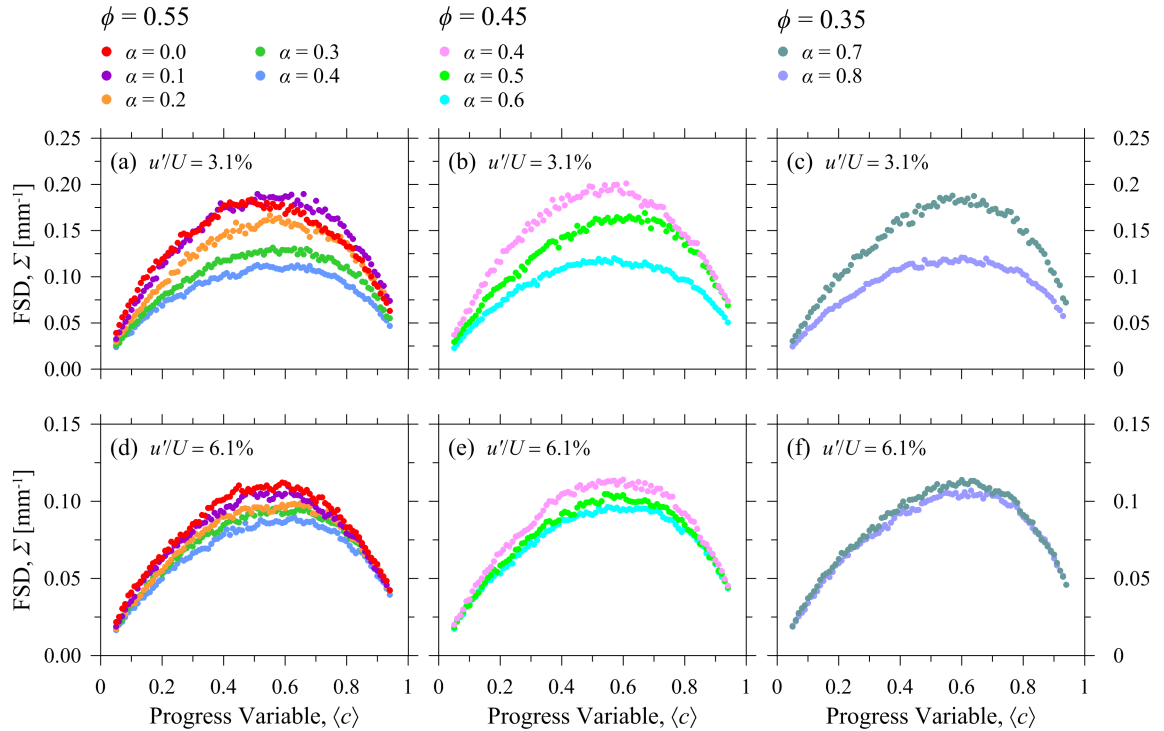


Figure 4 FSD for $u'/U = 3.1\%$ in (a), (b), and (c) and $u'/U = 6.1\%$ in (d), (e), and (f) for equivalence ratios $\phi = 0.55$, $\phi = 0.45$, and $\phi = 0.35$ respectively.

3.4 Curvature κ

Curvature data were obtained by fitting a cubic spline to instantaneous flame contours and calculated from $\kappa = (\dot{x}\ddot{y} - \dot{y}\ddot{x}) / (\dot{x}^2 + \dot{y}^2)^{3/2}$. The current study followed the convention that positive curvatures are convex towards the reactants and negative curvatures concave towards the reactants.

Length-weighted PDFs of curvature are shown in Figure 5 and are consistent with those reported for lean, CH_4/air turbulent V-flames of comparable Lewis numbers [8,16]. The slight bias towards positive curvatures and prominent negative tail is typical of cusped flames, and further supports the FSD results in section 3.3. The PDFs are also broader

for higher turbulence intensities as flame wrinkling increases with u' .

The profiles in (a) $\phi = 0.55$ showed a small yet repeatable progressive shift towards more positive curvatures with α_{H_2} , as the most probable curvature shifted from 0.12 mm to 0.18 mm for $\alpha_{H_2} = 0.0$ and $\alpha_{H_2} = 0.4$. This trend was more pronounced for leaner flames in (b) $\phi = 0.45$ and (c) $\phi = 0.35$, where the most probable curvature shifted from 0.12 mm to 0.20 mm, and 0.10 mm to 0.22 mm despite changes

in hydrogen fraction α_{H_2} of only 0.2 and 0.1 respectively. The profiles in (a), (b), and (c), also showed a small broadening with α_{H_2} as the probability of smaller negative curvatures increased. These trends are consistent with the increasingly cusped structures observed in Figure 1 and the gradual shift in bias of FSD profiles in Figure 4. They are attributed to the decrease in thermo-diffusive stability as α_{H_2} increases.

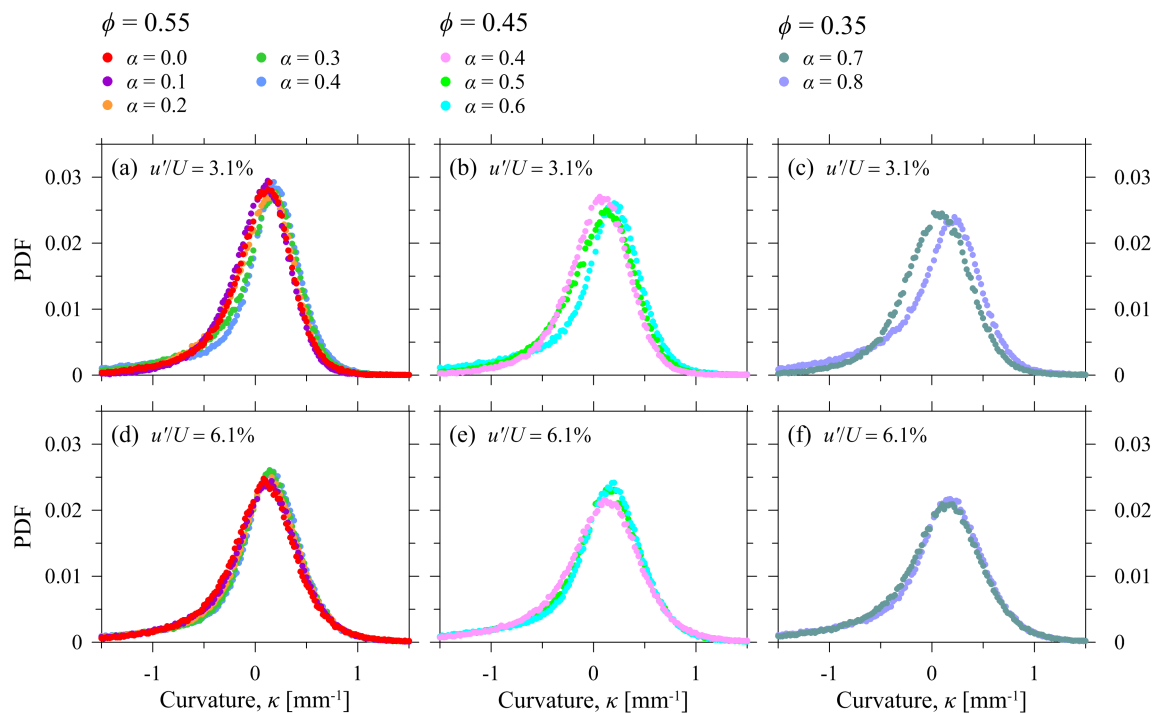


Figure 5 Curvature PDF's for (a) rich front supported, (b) rich back supported, and (c) lean back supported premixed and stratified flame conditions with a binning size of 0.02 mm

Flames propagating in higher turbulence intensity $u'/U = 6.1\%$ showed less variation in curvature. PDFs in (d), (e), and (f) showed near-negligible change in bias and broadening with α_{H_2} . This suggests that for the lean CH_4 - H_2 /air flames considered, flame topology and wrinkling scales become driven by flame/turbulence interactions more so than by thermo-diffusive effects at higher turbulence intensities.

4. Conclusions

The effect hydrogen enrichment on lean, CH_4 - H_2 /air turbulent V-flames was studied for equivalence ratios $\phi = 0.55$, $\phi = 0.45$, and $\phi = 0.35$ and turbulence intensities $u'/U = 3.1\%$ and 6.1% . Mie scattering images provided information on the topology of the flame front, and were studied for variations in turbulent flame propagation speed S_T , turbulent flame brush thickness δ_T , flame surface density Σ , and flame front curvature κ .

Hydrogen enrichment increased the turbulent flame propagation speed and turbulent flame brush

thickness of all flames considered. Flame surface density profiles showed a progressive shift towards the products as the volume fraction of H_2 increased. Curvature PDFs showed a bias towards positive curvatures with the volume fraction of H_2 . These trends were attributed to the presence of cusp-like structures of negative curvature along the flame front. As the volume fraction of H_2 increased, the reactant Lewis number decreased, and cusped structures were enhanced by thermo-diffusive effects.

5. References

- [1] C.G. Bauer, T.W. Forest, Int. J. Hydrogen Energy 26 (2001) 55.
- [2] C.G. Bauer, T.W. Forest, Int. J. Hydrogen Energy 26 (2001) 71.
- [3] F. Ma, Y. Wang, H. Liu, Y. Li, J. Wang, S. Zhao, Int. J. Hydrogen Energy 32 (2007) 5067.
- [4] F. Ma, Y. Wang, H. Liu, Y. Li, J. Wang, S. Ding, Int. J. Hydrogen Energy 33 (2008) 823.

- [5] G.S. Jackson, R. Sai, J.M. Plaia, C.M. Boggs, K.T. Kiger, *Combust. Flame* 132 (2003) 503.
- [6] S. Jain, D. Li, S.K. Aggarwal, *Int. J. Hydrogen Energy* 38 (2013) 4163.
- [7] H. Guo, B. Tayebi, C. Galizzi, D. Escudié, *Int. J. Hydrogen Energy* 35 (2010) 11342.
- [8] P. Anselmo-Filho, S. Hochgreb, R.S. Barlow, R.S. Cant, *Proc. Combust. Inst.* 32 (2009) 1763.
- [9] P.C. Vena, B. Deschamps, G.J. Smallwood, M.R. Johnson, *Proc. Combust. Inst.* 33 (2011) 1551.
- [10] J.B. Bell, R.K. Cheng, M.S. Day, I.G. Shepherd, *Proc. Combust. Inst.* 31 I (2007) 1309.
- [11] N. Peters, *Turbulent Combustion*, Cambridge University Press, 2000.
- [12] E.R. Hawkes, J.H. Chen, *Combust. Flame* 138 (2004) 242.
- [13] F.A. Williams, *Combustion Theory: The Fundamental Theory of Chemically Reacting Flow Systems*, 2nd ed., The Benjamin/Cummings Publishing Company Inc., 1985.
- [14] B.M. Deschamps, G.J. Smallwood, J. Prieur, D.R. Snelling, O.L. Gulder, *Proc. Combust. Inst.* 26 (1996) 427.
- [15] S.B. Pope, *Int. J. Eng. Sci.* 26 (1988) 445.
- [16] I.G. Shepherd, *Proc. Combust. Inst.* 26 (1996) 373.